# Full spectrum fitting method: a new approach for instantaneous phosphor thermometry in harsh environments

Valentin Lechner, Christopher Betrancourt, Clément Mirat, Philippe Scouflaire, Sébastien Ducruix

▶ **To cite this version:**

Valentin Lechner, Christopher Betrancourt, Clément Mirat, Philippe Scouflaire, Sébastien Ducruix. Full spectrum fitting method: a new approach for instantaneous phosphor thermometry in harsh environments. Experiments in Fluids, 2022, 63 (7), pp.110. 10.1007/s00348-022-03461-2 . hal-04311086

**HAL Id: hal-04311086**
**https://hal.science/hal-04311086v1**

Submitted on 10 Oct 2024

**HAL** is a multi-disciplinary open access archive for the deposit and dissemination of scientific research documents, whether they are published or not. The documents may come from teaching and research institutions in France or abroad, or from public or private research centers.

L'archive ouverte pluridisciplinaire **HAL**, est destinée au dépôt et à la diffusion de documents scientifiques de niveau recherche, publiés ou non, émanant des établissements d'enseignement et de recherche français ou étrangers, des laboratoires publics ou privés.

**Experiments in Fluids manuscript No.**
(will be inserted by the editor)

# Full Spectrum Fitting method: a new approach for instantaneous phosphor thermometry in harsh environments

**Valentin Lechner · Christopher Betrancourt · Clement Mirat · Philippe Scouflaire · Sébastien Ducruix**

Received: date / Accepted: date

**Abstract** This paper proposes a new approach for the post-treatment of Laser Induced Phosphorescence (LIP) signals for instantaneous surface temperature measurements. LIP is a semi-invasive optical diagnostic based on coated thermographic phosphor surfaces, emitting a temperature-dependent signal under laser irradiation. The so-called "Full Spectrum Fitting method" (FSF method) uses the dependence of the entire phosphorescence spectrum with temperature. $Mg_{3.5}FGeO_5$:Mn phosphorescence spectra are acquired to build a database at each kelvin in a temperature range from 100 K to 900 K with a unique set of experimental acquisition parameters. The constituted database is used to retrieve a single-shot temperature measurement using a least mean square algorithm. Statistical studies show excellent performance of the FSF method for single-shot temperature determination with a 12 K precision and no significant influence of temperature. In the same conditions, the error on temperature raises with the temperature with the more common Intensity Ratio method (IR method). Since it is difficult or even impossible to know the exact energy exciting the phosphor in harsh high-absorbing environments, an investigation on the influence of the laser fluence is carried out. It shows dependencies on the phosphorescence spectrum leading to errors during the temperature determination when the calibration and the measurement are not performed at the same laser fluence. Acquiring multiple databases at different laser fluences and systematically checking them with the least mean square algorithm allows being nearly independent of the laser fluence with the FSF method.

**Keywords** laser induced phosphorescence · thermographic phosphors · surface thermometry · instantaneous measurements

V. Lechner
CNES, Direction Technique et Numérique, Paris, France

V. Lechner · C. Betrancourt · C. Mirat · P. Scouflaire · S. Ducruix
Université Paris-Saclay, CNRS, CentraleSupélec, Laboratoire EM2C, Gif-sur-Yvette, France

E-mail: christopher.betrancourt@centralesupelec.fr

## 1 Introduction

Surface temperature knowledge is essential in energy converting systems such as turbines, rocket engines, nuclear reactors, or glass melting furnaces. Their efficiency and lifetime are strongly dependent on wall temperature.

In combustors, the wall temperature may trigger transitions between different flame topologies (Guiberti et al. 2015). Mercier et al. (2016) and Koren et al. (2018) illustrated this coupling by Large Eddy Simulations (LES) taking into account experimental thermal boundary conditions. Its fine control is highly valuable in the combustor design. More accurate and resolved experimental surface temperature measurements are necessary to improve its understanding.

In the combustion research field, experiments are often performed in the transient thermal regime and in a short period of time to protect the setup. For example, in subscale rocket engines (Vingert et al. 2016; Lux et al. 2006; Salgues et al. 2006), the duration of operation does not exceed dozens of seconds because of the extreme conditions: a pressure up to 70 bar (Vingert et al. 2016) and a surface temperature from 120 K to 800 K. Some burners can even reach a maximal surface temperature up to 1200 K (Degenève et al. 2019). To perform accurate and temporally resolved surface temperature measurements on such experimental conditions is a challenging task.

Among the various experimental techniques developed to measure the temperature near a surface, thermocouples

are frequently used. They are sensitive to a wide range of temperatures, and some of them can capture fast temperature changes (Heichal et al. 2005; Marr et al. 2010). However, they are invasive probes, and their implementation needs to be planned at the design level of the investigated system.

Pyrometry is another possibility based on the measurement of the surface radiation. It requires the exact knowledge of the surface emissivity, which is difficult to assess and may change during operation. Moreover, radiations from flames or other bodies may affect the measurement.

Heat-sensitive paints allow an estimation of the peak temperature through their irreversible change of color (Lempereur et al. 2008). They are inappropriate for time-resolved measurements in high-temperature combustion environments.

Laser Induced Phosphorescence (LIP) thermometry is an established method to measure surface temperature. The readers can refer to many reviews on the principles and applications of the technique (Allison and Gillies 1997; Khalid and Kontis 2008; Chambers and Clarke 2009; Aldén et al. 2011; Brübach et al. 2013; Dramićanin 2020). The fundamental principles of the two main experimental approaches to retrieve the temperature and their limitations for combustion environments are resumed in this introduction.

Surfaces of interest are coated with a thermographic phosphor, an activator doped ceramic (Brübach et al. 2013), which emits a phosphorescence signal under laser irradiation. The temporal and spectral properties of this signal are temperature-dependent. These properties are used to determine an unknown temperature through an appropriate calibration. Two approaches are mainly used for the determination of the temperature. On the one hand, the lifetime method takes advantage of the temperature dependence of the exponential decrease of the phosphorescence signal after laser excitation (McCormack 1981). The function of the decay time with the temperature, $\tau(T)$, is a calibration curve. Depending on the phosphor used, cryogenic (Beshears et al. 1990; Cates et al. 1997) to high temperatures (Cates et al. 2003) can be measured, and the decay time can vary in few decades, from milliseconds to microseconds. On the other hand, the spectral or intensity ratio method takes advantage of the emission spectrum temperature dependence (Goss et al. 1989). The calibration curve is built by computing the intensity ratio, $R(T)$, from two spectral bands of the spectrum. Detectors with proper filters are used to collect the light from these two regions of the spectrum. This method is preferably used for 2D (Bizzak and Chyu 1994; Omrane et al. 2004a) or even fluid temperature measurements with dispersed phosphor particles (Abram et al. 2018; Fond et al. 2012; Abram et al. 2015).

For the targeted applications of this paper, i.e., harsh combustion environments with temperature gradients, the lifetime method with a phosphor with a wide sensitive temperature range and short lifetime is often preferred. However, to cover an extensive temperature range of 800 K involving four orders of magnitude in terms of lifetime (Degenève et al. 2018), it demands a detector with fast-changing settings or with a high dynamic range at a given set. Thus, automatic routines have been imagined to extend the dynamic temperature range (Degenève et al. 2018; Abou Nada et al. 2016; 2014) but limit the instantaneous temperature sampling rate at a few hertz. High-speed cameras can also be used for this purpose (Kissel et al. 2009; Someya et al. 2011; 2013) while providing two-dimensional measurements without changing the detector settings. Measurements with good precision, up to 5 K single-pixel single-shot standard deviation on a temperature range from 300 K to 900 K have been demonstrated (Kissel et al. 2009).

Instantaneous measurements are still challenging for both methods, especially in combustion applications. In turbulent flames, the thermal background fluctuations and sometimes the presence of soot (radiating and deposing on walls) make it necessary to use average signals to obtain a better signal-to-noise ratio (Nau et al. 2017; Arndt et al. 2020). This performance has been achieved in rapid compression machine applications with CMOS cameras (Someya et al. 2011; 2013) but on a limited temperature range of less than 200 K.

In addition to the difficulty of instantaneous measurements, accuracy and uncertainty depend on the experimental setup sensitivity. For example, the intensity ratio method is sensitive to the optical alignment (Fuhrmann et al. 2013) whereas the lifetime method needs special attention to fluorescence interferences (Mendieta et al. 2019). Moreover, many authors agree that the excitation energy can be a source for stochastic errors in the temperature determination for both methods (Hertle et al. 2020; Abou Nada et al. 2016; Kueh et al. 2015; Fond et al. 2015; Abram et al. 2015; Abou Nada et al. 2014; Fuhrmann et al. 2013; Heeg and Jenkins 2013; Fond et al. 2012; Fuhrmann et al. 2011; Lindén et al. 2009; Brübach et al. 2008; Feist 2001; Imanaga et al. 1979). This is a matter of concern in high-absorbing environments like turbulent sooting flames where the exact energy amount exciting the phosphor can be lower than the one used for the calibration.

This brief overview underlines the main challenges to measure instantaneous surface temperature by conventional LIP methods in a combustion environment.

The present work proposes a new approach for instantaneous phosphor thermometry in harsh environments with good precision based on a spectral method proposed by Vander Wal et al. (1999). This approach, named "Full Spectrum Fitting method" (FSF method), allows to:

- exploit single-shot measurements;
- cover a wide temperature range (800 K) without a priori knowledge of the temperature;

- track the temperature at 10 Hz in transient thermal regimes;
- work with a unique set of experimental parameters;
- be independent of the excitation energy;
- perform point measurements in experiments with limited optical access.

The thermographic phosphor $Mg_{3.5}FGeO_5$:Mn is selected for this work for its known excellent spectral sensitivity on a wide temperature range (Vander Wal et al. 1999; Omrane et al. 2004b; Brübach et al. 2008; Abou Nada et al. 2014).

The Intensity Ratio method (IR method) and the Full Spectrum Fitting method (FSF method) are compared through statistical analysis on single-shot temperature determination and laser fluence effects. These analyses demonstrate the main benefit of the FSF method compared to the IR method for instantaneous surface temperature measurements.

## 2 Choice of the phosphor

The purpose of this work requires a thermographic phosphor: 1) with good spectral dynamics on a wide range of temperatures and 2) a short lifetime to retrieve the temporal temperature evolution of the investigated system.

The thermographic phosphor $Mg_{3.5}FGeO_5$:Mn satisfies the first condition to apply the FSF method as illustrated in figure 1. $Mg_{3.5}FGeO_5$:Mn is sensitive from cryogenic to high temperatures (from 8 K (Cates et al. 1997) to 1200 K (Degenève et al. 2019)). The spectra from 100 K to 900 K display an intense peak around 660 nm, shifting as a function of the temperature. The 630 nm peak increases relatively to the 660 nm one in intensity while both linewidths expand with temperature. These lines are usually used for the IR method. As seen by Vander Wal et al. (1999), starting from 700 K, another broad line appears under 580 nm and increases with temperature.

The phosphorescence signal lifetime is about a few milliseconds at ambient temperature and hundreds of nanoseconds at high temperatures, satisfying the second condition to track the temporal temperature evolution.

## 3 Experimental approach

A $Mg_{3.5}FGeO_5$:Mn phosphor coating is applied on a thermocouple and excited with a pulsed laser at 355 nm. Phosphorescence spectra are acquired with an imaging spectrometer at each kelvin from 100 K to 900 K. The spectrum is stored with its temperature at each laser pulse. Figure 2 shows the experimental setup, which is described in the following paragraphs.

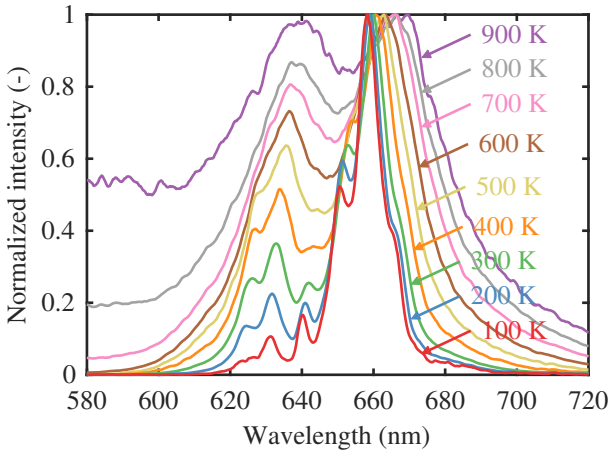


**Fig. 1** Normalized average $Mg_{3.5}FGeO_5$:Mn phosphorescence spectra at different temperatures after laser excitation at 355 nm with a fluence of 64 mJ cm$^{-2}$.

### 3.1 Phosphor coating

The thermographic phosphor powder $Mg_{3.5}FGeO_5$:Mn (Phosphor Technology, EQD25/NU1) is mixed with an industrial binder (ZYP Coatings, HPC Binder). A dilution water volume corresponding to 10 % of the binder volume is added. This mixture is then coated with an airbrush (Aerographe Services, Utopia C05) with ten layers. Each layer is dried at ambient air conditions for a few minutes. The thickness has been estimated not to exceed 100 µm in a previous study in the laboratory by Guiberti et al. (2014). The coating is applied on a K-type sheathed thermocouple with a diameter of 1.5 mm.

### 3.2 Temperature control

The coated thermocouple is placed above two complementary devices to access a temperature range from 100 K to 900 K. A home-made heat exchanger is used for cryogenic temperatures from 100 K to 300 K. The exchanger is fed by gaseous nitrogen at ambient pressure and immersed in a Dewar filled with liquid nitrogen. Dry nitrogen is used instead of air (potentially humid) to prevent the creation of an ice plug in the exchanger. According to Brübach et al. (2007), using gaseous nitrogen should not affect the phosphorescence signal. The coated thermocouple is positioned in the cold flow of gaseous nitrogen at the exit of the exchanger. The temperature is decreased from ambient to 100 K. The exchanger is replaced by an air electric heater (Leister, CH-6056, 2850W) to access the temperature range from ambient up to 900 K. The heating increase rate is adjusted at $\sim$ 0.2 K s$^{-1}$ in this work, low enough to enable a homogenous temperature inside the phosphor coating during

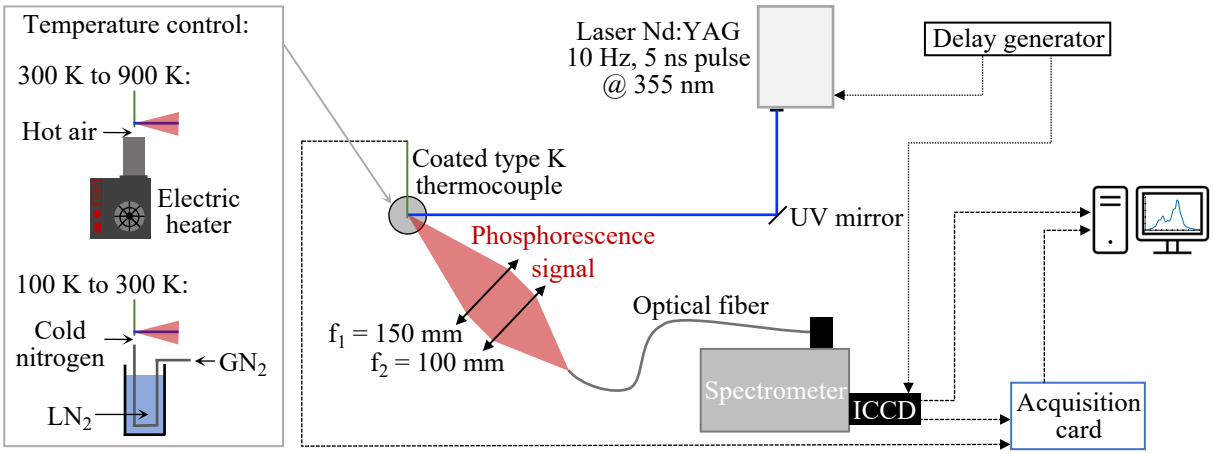


**Fig. 2** Experimental setup for phosphorescence spectra acquisition from 100 K to 900 K.

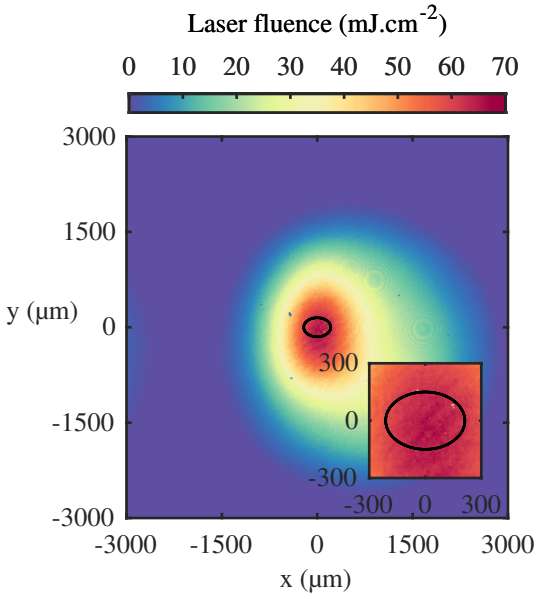


**Fig. 3** Fluence distribution at an average energy of 3 mJ. The black ellipse represents the spot looked at with the phosphorescence detection optics.

the phosphorescence spectra acquisition (10 Hz) (Guiberti 2015; Degenève 2020).

### 3.3 Excitation source

The phosphor coating is excited at 355 nm using the 3rd harmonic of a Nd:YAG laser (Continuum, Minilite ML II) triggered at 10 Hz with a 5 ns width pulse. The pulse energy is adjusted by the included attenuator and recorded with a pyroelectric energy detector (Gentech-EO, QE25-SP-S-MB). The maximum laser energy is 5 mJ per pulse with a standard deviation of 3 % at 355 nm. Ten energy levels are used in this study, starting from 0.5 mJ up to 5 mJ with a 0.5 mJ step. The laser beam profile is recorded with a camera (Gentec BEAMAGE-4M beam profiler) and converted in laser fluence for each pixel, knowing the size of the surface looked at with the detection optics (section 3.4). It has been controlled that the laser energy changes neither the energy distribution of the beam, nor the laser fluence. For example, figure 3 shows the fluence distribution obtained at 3 mJ. The overall distribution is slightly elliptic but homogeneous in the spot looked at with the detection optics (black ellipse). Thus, the average fluence in this surface is determined, leading to a value of 64 mJ cm$^{-2}$ for a 3 mJ laser energy.

### 3.4 Phosphorescence detection and spectra acquisition

A telescope oriented at 45° of the laser path and locked on the laser beam center is used to collect the phosphorescence signal. It is composed of two two-inch achromatic lenses ($f_1 = 150$ mm and $f_2 = 100$ mm, Thorlabs, AC508-150-A, and AC508-100-A). The light is then focused on a 200 µm multimode optical fiber leading to the entrance slit of a spectrometer, which slit width matches the fiber diameter. This optical assembly acts as a spatial filter limiting unwanted light. With a 1.5 magnification, the phosphorescence signal is collected from an elliptic surface (300 µm minor axis and 424 µm major axis) with a homogeneous fluence distribution as illustrated in figure 3. The phosphorescence signal is imaged at 10 Hz with a spectrometer (Princeton Instrument, Spectra Pro 500i, $f = 500$ mm, gratting of 150 grooves mm$^{-1}$) coupled with an intensified CCD camera (Princeton Instrument, Pi-Max, 512 x 512 pixel$^2$) covering a spectral range of 160 nm centered at $\lambda = 650$ nm with a resolution of 0.3 nm pixel$^{-1}$. The chosen wavelength resolution allows capturing enough details in the spectrum to distinguish them at each temperature (see figure 1). The spectra present in this work are not calibrated in intensity. The laser and the spectrometer are synchronized with an external delay generator

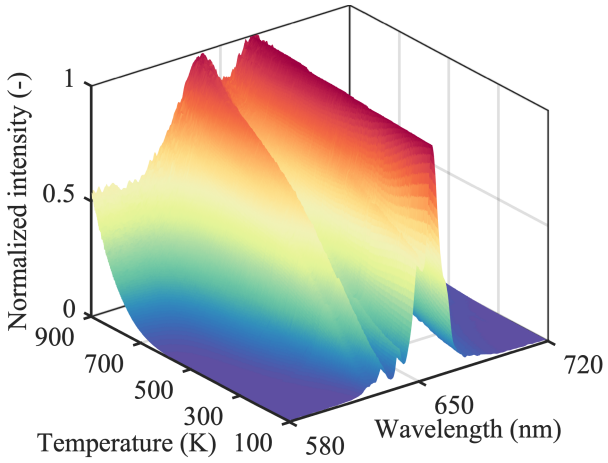


**Fig. 4** Database constituted of normalized average $Mg_{3.5}FGeO_5$:Mn phosphorescence spectra after laser excitation at 64 mJ cm$^{-2}$ laser fluence.

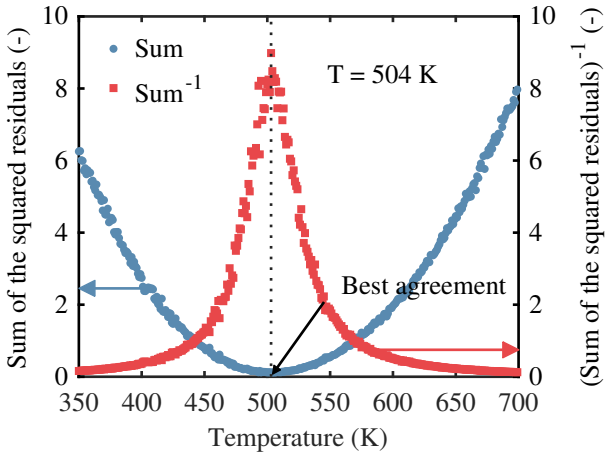


**Fig. 5** Example of the sum of the squared residuals and its inverse between a single-shot spectrum and average spectra at 64 mJ cm$^{-2}$ laser fluence as a function of temperature.

(BNC, Model 577 Pulse Generator). A 50 ns delay between the laser pulse and the camera exposition is set to avoid any laser contribution and prevent potential interferences from fluorescence sources as reported by Mendieta et al. (2019). The exposure time is set to 30 µs. These parameters are kept constant for temperatures from 100 K to 900 K.

No effect of angle or target distance on the shape of the phosphorescence spectrum has been identified as long as the laser energy is constant, and the telescope is locked on the laser beam center. However, the absolute signal intensity could change and affect the precision of the method, so special attention is required to have a good signal-to-noise ratio.

Using a telescope containing the optics coupled with an optical fiber is particularly well-adapted for point measurements in experiments with limited optical access and makes optical alignments easier

### 3.5 Databases acquisition

A LabVIEW program records the temperature and the corresponding spectrum thanks to an acquisition card (National Instruments, PCI-6111). An average spectrum is computed at each kelvin and corrected for the background noise. A 3-order Savitzky-Golay smoothing filter with a moving window of 13 points is applied. Figure 4 shows the constituted database at 64 mJ cm$^{-2}$ laser fluence. Ten databases have been acquired by varying the laser fluences from 11 to 106 mJ cm$^{-2}$.

## 4 Temperature determination: data inversion processes

Instantaneous temperatures are determined from single-shot measurements using two data inversion processes: the new approach named Full Spectrum Fitting method (FSF method) and the well-established Intensity Ratio method (IR method).

In agreement with the paper objectives, a unique set of acquisition parameters is chosen for the FSF method to perform measurements in transient thermal regimes on a wide range without a priori knowledge of the temperature. The following comparison with the IR method is thus performed in the same experimental conditions.

### 4.1 Full Spectrum Fitting method

The FSF method is based on the pioneering work of Vander Wal et al. (1999), who took advantage of the full spectrum to determine the temperature. They constituted a database of $Mg_{3.5}FGeO_5$:Mn phosphorescence spectra at known temperatures ranging from 473 K to 923 K and different laser fluences. Then, the average spectrum is inverted to retrieve the temperature using a custom general neural algorithm to compare the measurement spectrum from those in the database. The present work takes up the use of the full spectrum dependence on temperature and proposed several novelties and clarification on:

- a simplified data analysis process to retrieve the instantaneous temperature, independently of the laser fluence knowledge (section 5.2) as well as a precision analysis process (section 5);
- an extended temperature range from 100 K to 900 K for the FSF method application.

Thus, the so-called "Full Spectrum Fitting method" is based on the full phosphorescence spectrum dependence on temperature instead of on narrow bands. A spectra database

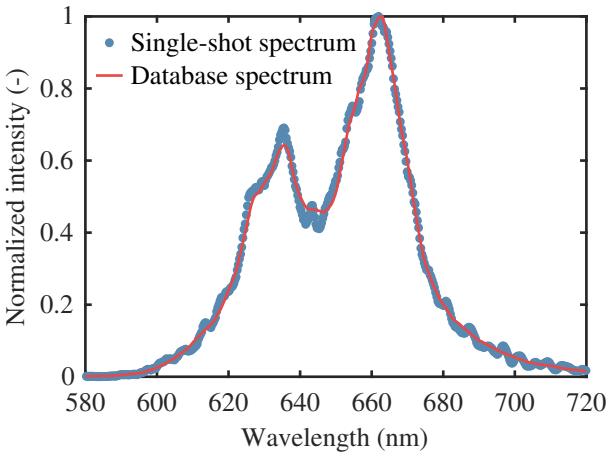


**Fig. 6** Normalized single-shot spectrum and average spectrum at 504 K extracted from the database at 64 mJ cm$^{-2}$ laser fluence using the least mean square algorithm.

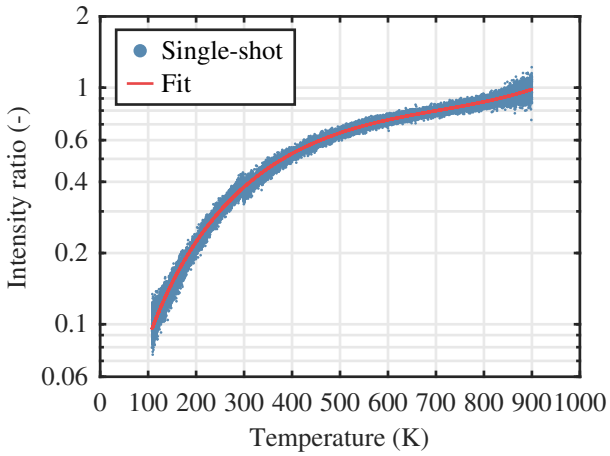


**Fig. 7** Fitted calibration curve (red line) of the intensity ratio computed with the database of average spectra and scattered intensity ratios of single-shots (blue dots) at 64 mJ cm$^{-2}$ laser fluence.

at known temperatures and laser fluences replaces the calibration curve necessary for the IR method (section 4.2). Then, a spectrum measured at an unknown temperature can be retrieved using this database and the following straightforward approach.

As a first step, a classical least mean square algorithm is chosen to fulfill this task. The algorithm computes the sum of the squares of the residuals between the single-shot spectrum and the average spectra in the database. This sum describes a parabolic curve as a function of the temperature, as illustrated in figure 5. The target temperature corresponds to the maximum of the inverse of this function.

This procedure is illustrated in figures 5 and 6 for a single-shot spectrum acquired at 64 mJ cm$^{-2}$. The best match corresponds to the maximum of this curve, 504 K, for this example. The corresponding spectrum from the database and the single-shot one are plotted together in figure 6 showing a very good agreement.

The laser fluence dependence on spectra will be considered in the dedicated section (5.2).

### 4.2 Intensity Ratio method

The IR method takes advantage of the temperature-dependent changes of the emission spectrum (Goss et al. 1989) (see figure 1). A ratio $R(T)$ is computed at each temperature by dividing intensities from two spectral regions $\Delta\lambda_1$ and $\Delta\lambda_2$, acquired with two adequate filters:

$$R(T,\Delta\lambda_1,\Delta\lambda_2) = \frac{\int_{\Delta\lambda_1} I(\lambda,T)d\lambda}{\int_{\Delta\lambda_2} I(\lambda,T)d\lambda}. \quad (1)$$

$I(\lambda,T)$ denotes the absolute phosphorescence intensity at temperature $T$ and wavelength $\lambda$. The calibration curve $R(T)$ is built experimentally by computing this ratio at known temperatures and fitting a polynomial function. An unknown temperature is determined by computing the intensity ratio from its phosphorescence signal and reversing this function. The accuracy and sensitivity of the IR method highly depend on the phosphor characteristics and the critical choice of the spectral collection filters $\Delta\lambda_1$ and $\Delta\lambda_2$ (Abram et al. 2018). For phosphorescence spectra with discrete peaks, filters are often centered on them (Fuhrmann et al. 2013; Omrane et al. 2004a). Optimization procedures may be used to find filters that improve the precision but in limited temperature ranges (Petit et al. 2022; Särner et al. 2008a).

In this work, a calibration curve $R(T)$ is built by computing a ratio from 100 K to 900 K for each average spectrum in the database with $\Delta\lambda_1 = [633 \pm 5]$ nm and $\Delta\lambda_2 = [660 \pm 5]$ nm to reproduce the usual experimental conditions (Fuhrmann et al. 2013). The calibration curve shown in figure 7 is finally obtained by fitting a 5-order polynomial function on $R(T)$.

## 5 Single-shot precision evaluation

A comparative statistical study is conducted for the FSF method and IR method on instantaneous temperature determination. The laser fluence dependence of $Mg_{3.5}FGeO_5$:Mn phosphorescence spectra and its impact on the temperature determination are illustrated for both methods. A methodology is finally proposed to minimize the laser fluence dependency and the associated error on the temperature determination with the Full Spectrum Fitting method.

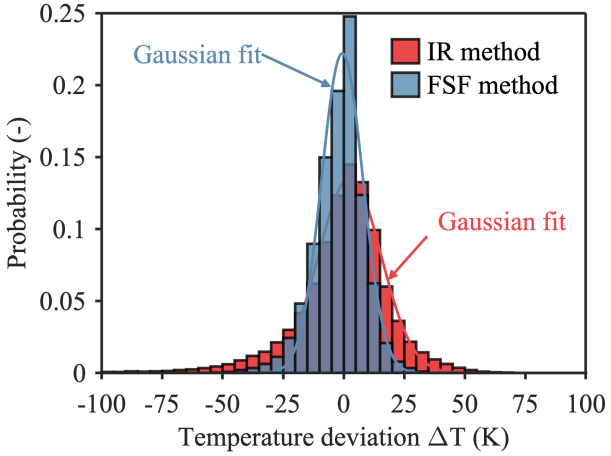


**Fig. 8** Histograms of the temperature deviation $\Delta T = T_{found} - T_{recorded}$ obtained with the FSF method and the IR method at 64 mJ cm$^{-2}$ laser fluence. Gaussian fits parameters: average temperature deviations of $\overline{\Delta T}_{FSF} = -0.59$ K and $\overline{\Delta T}_{IR} = 2.52$ K, standard deviations of $\sigma_{\Delta T,FSF} = 12.11$ K and $\sigma_{\Delta T,IR} = 18.23$ K.

### 5.1 Single-shot precision

Conventionally, the single-shot precision is appreciated regarding the standard deviation associated with average signals used to build the calibration curve (Fuhrmann et al. 2011). Other works conducted statistical studies to determine the single-shot precision at specific temperatures either for the lifetime or intensity ratio method (Abram et al. 2013; Lawrence et al. 2013; Fond et al. 2012).

It should be noted that the spacing of the database is a limiting factor for the accuracy, 1 K in the present case. The lifetime and the intensity ratio methods are not subject to this limitation because the calibration curve is obtained by fitting the measurements. The spacing between those measurements can be higher than with the FSF method as far as the fitted curve is not too far away from them. Nonetheless, with the FSF method, one could also imagine fitting a calibration curve as a function of the temperature at each wavelength of the spectra. This latter option has not been selected in this work to stay as close as possible to the measurements.

In this study, the temperature determination precision from instantaneous measurements is obtained for the FSF and IR methods. For this purpose, both approaches are applied to determine the temperature of the hundreds of thousands single-shot measurements recorded with their temperature and laser fluence. Then, the "temperature deviation" is defined as follow: $\Delta T = T_{found} - T_{recorded}$.

The distribution of temperature deviation for each instantaneous measurement is plotted in histograms. Figure 8 illustrates a typical result at 64 mJ cm$^{-2}$ laser fluence for both methods. The IR method displays a higher dispersion than the FSF method with respectively an average deviation

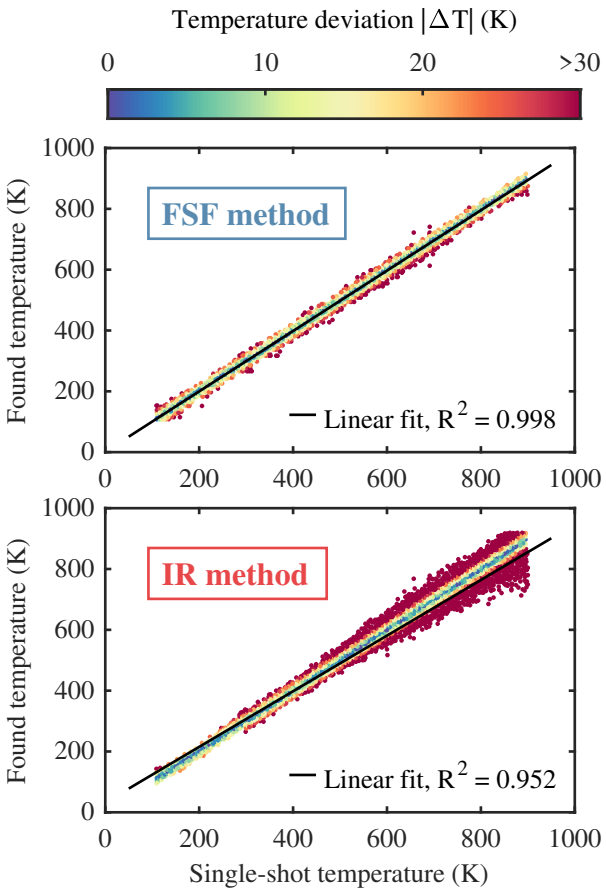


**Fig. 9** Scatter plots between the temperature found with the FSF method (top) and the IR method (bottom) and the recorded single-shot temperature at 64 mJ cm$^{-2}$ laser fluence. The color indicates the absolute temperature deviation $|\Delta T| = |T_{found} - T_{recorded}|$.

$\overline{\Delta T}_{IR} = 2.52$ K, $\overline{\Delta T}_{FSF} = -0.59$ K and a standard deviation $\sigma_{\Delta T,IR} = 18.23$ K, $\sigma_{\Delta T,FSF} = 12.11$ K. In detail, the FSF method displays a temperature deviation smaller than 5 K for around 45 % of the single-shot spectra and between 5 K and 10 K for 30 % of them. The maximum error is beyond 50 K for only 0.17 % of them. The IR method shows a temperature deviation smaller than 5 K for only 27 % of the measurements and almost the same between 5 K and 10 K. The maximum error is beyond 50 K for almost 10 % of the statistical sample.

This global analysis is completed by an evaluation of the precision of these two methods at each temperature. Figure 9 gathers the temperature deviation for the 64 mJ cm$^{-2}$ laser fluence database. Each dot is colored depending on the absolute deviation with the single-shot temperature: $|\Delta T|$. For the FSF method, a linear fit is applied with $R^2 = 0.998$, meaning minimal dispersion of the results. Moreover, the error on the temperature determination is equivalent for all temperatures. The dispersion of the results for the IR method is more important than with the FSF method and increases

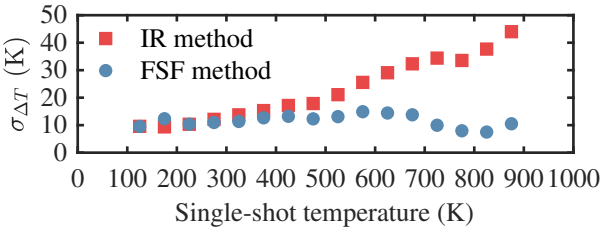


**Fig. 10** Standard deviation $\sigma_{\Delta T}$ as a function of the single-shot temperature for the FSF method and the IR method at 64 mJ cm$^{-2}$ laser fluence.

with temperature. This is confirmed by the lower coefficient of determination $R^2 = 0.952$. In the worst cases, an error of several dozens of kelvins appears with the IR method compared with an error of a few kelvins with the FSF method.

The standard deviation can be determined as a function of the temperature for both methods. Every 50 K, from 100 K to 900 K, the temperature deviation is determined for all the single-shot spectra binning on 50 K. Then, the standard deviation is obtained from a Gaussian fit.

Figure 10 shows that both methods present the same evolution between 100 K and 500 K, changing from 10 K to 15 K. After 500 K, the single-shot dispersion becomes worse with the IR method, with a standard deviation up to 45 K at 900 K. On the other hand, it hardly changes between 500 K and 700 K with the FSF method and becomes better after 700 K. Indeed, as seen in figure 1, spectra are more distinguishable from one another after 700 K allowing better performances of the least mean square algorithm. Thus, the precision on single-shots is below 10 K between 700 K and 900 K with the FSF method."

A global analysis is also performed at nine other laser fluences from 11 mJ cm$^{-2}$ to 106 mJ cm$^{-2}$. For each laser fluence it was verified that the evolution of the dispersion as a function of temperature is similar to that observed at 64 mJ cm$^{-2}$. The average temperature deviation $\overline{\Delta T}$ and the standard deviation $\sigma_{\Delta T}$ are determined for each laser fluence and both methods and gathered in figure 11. The evolution with the laser fluence is different according to the method. Whereas the temperature deviation decreases with the fluence until reaching a plateau at 1 K for the FSF method, it increases with the fluence until reaching a plateau at 2.5 K for the IR method.

The standard deviation is maximum when the fluence is low. Then it decreases when the fluence increases for both methods. It reaches a plateau for the FSF method at 53 mJ cm$^{-2}$. It gets a minimum before rising for the IR method. This means that it is preferable to put the laser fluence at a mid-value to obtain a lower dispersion of the results. The FSF method reaches a plateau both for the standard deviation and the average temperature deviation. It would be judicious to be at the beginning of the plateau since

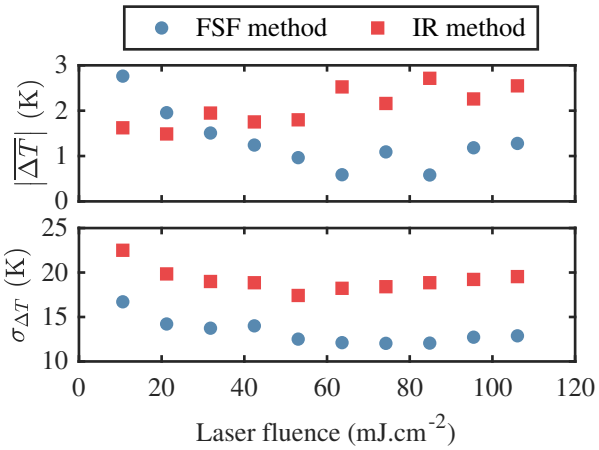


**Fig. 11** Absolute average temperature deviation $|\overline{\Delta T}|$ (top) and associated standard deviation $\sigma_{\Delta T}$ (bottom) as a function of laser fluence determined with the FSF method and the IR method.

non-linear phenomena could happen, degradation or warming of the coating. Anyway, the standard deviation with the FSF method is always lower than with the IR method meaning a more robust and efficient way for determining single-shot temperatures in a wide range of temperatures. These statistical studies show that the precision on single-shot measurements is better with the FSF method from 100 K to 900 K in well-controlled conditions.

### 5.2 Laser fluence effects on temperature determination

In absorbing environments, the laser fluence exciting the phosphor can be lower than the calibration. It can lead to potential errors in the temperature determination, particularly for thermographic phosphors which are sensitive to laser fluence. In this section, the impact of laser fluence dependence of $Mg_{3.5}FGeO_5$:Mn on temperature determination by IR and FSF methods are quantified.

• Effects on spectra and intensity ratio:

This section studies the effect of laser fluence on the phosphor response and the database and calibration curve.

Increasing the laser fluence increases the phosphorescence absolute intensity (not shown here). This tendency is helpful for FSF and IR methods to reach a good signal-to-noise ratio. This option must be used with caution regarding the possible induced damage of the coating (Lindén et al. 2009) and/or increase of the local temperature (Heeg and Jenkins 2013; Fuhrmann et al. 2011). Besides, the laser fluence must be chosen judiciously as demonstrated in section 5.1.

Figure 12 shows average spectra at different temperatures extracted from the databases obtained at 21, 42, 64, 85

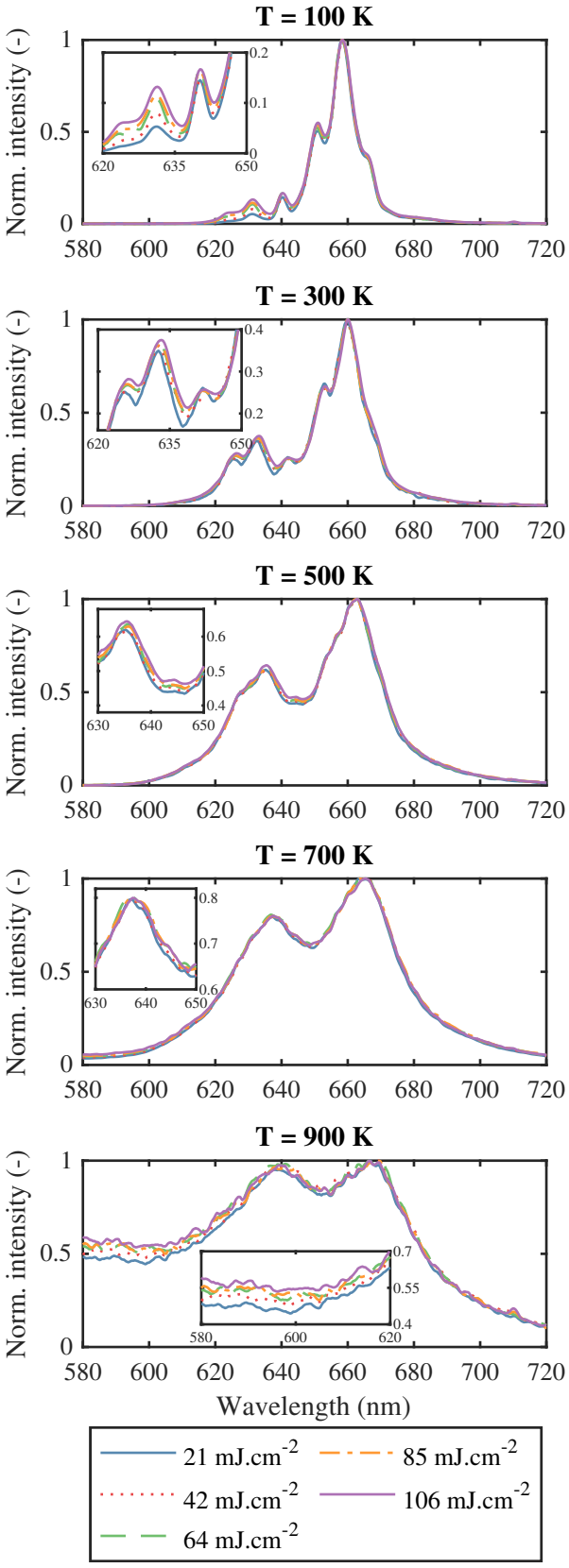


**Fig. 12** Normalized average $Mg_{3.5}FGeO_5$:Mn phosphorescence spectra at different temperatures and laser fluences. Spectra from only five out of the ten databases are shown to gain visibility.

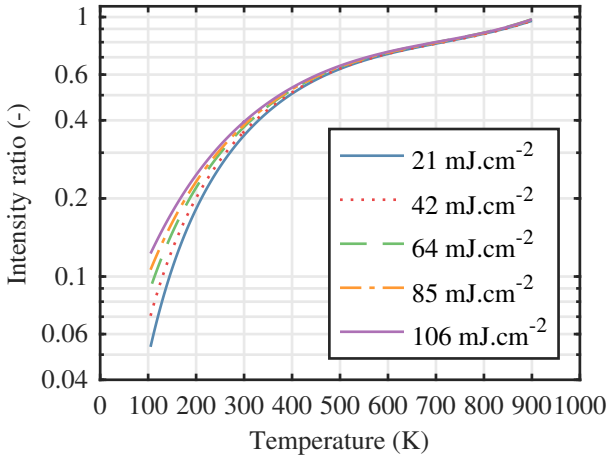


**Fig. 13** Calibration curves (fit) of the intensity ratio computed with the database of average spectra at different laser fluences. Only five out of the ten calibration curves are shown to gain visibility.

and 106 mJ $cm^{-2}$ laser fluences. Note that spectra at 900 K are a bit noisier due to the intensity decrease resulting in a lower signal-to-noise ratio. In contrast, the absolute intensity at 100 K is only slightly weaker than at 300 K. Figure 12 shows that fluence has no impact on the phoshpor response between 650 and 720 nm for all temperatures studied. Below this band, the effect of the laser fluence is more important at low temperatures. There is a strong dependency at 100 K, especially with the 630 nm emission band. The relative intensity of the 630 nm emission band increases with the laser fluence but not monotonously with temperature. Indeed, the difference between spectra becomes negligible while increasing temperature. A noticeable difference is visible at 900 K, although spectra are noisier. At high temperatures, the laser fluence dependence may be more important below the 580 nm wavelength. Thus, the $Mg_{3.5}FGeO_5$:Mn phosphorescence spectrum is not entirely independent on the laser fluence.

The effect of the fluence on the $Mg_{3.5}FGeO_5$:Mn response is reflected in its calibration curve. Figure 13 shows the evolution of the intensity ratio as a function of temperature at five laser fluences. Once again, there is a strong dependence at low temperatures, as seen on spectra around the 630 nm emission band (figure 12). The ratio increases by 192 % between 11 mJ $cm^{-2}$ and 106 mJ $cm^{-2}$ at 100 K, to reach only 3 % at 500 K. This evolution could lead to errors in the temperature determination if the laser fluence is different during the measurement and the calibration. Thus, the maximal temperature shift is 56 K at 100 K, and tends toward 15 K for temperatures above 500 K. However, it does not mean that the temperature error for single-shots is lower at high temperatures. Indeed, the dispersion of the single-shot ratio is much higher at high temperatures than at low ones (figure 7). This analysis shows that the temperature error can be higher at low temperatures if the laser fluence is

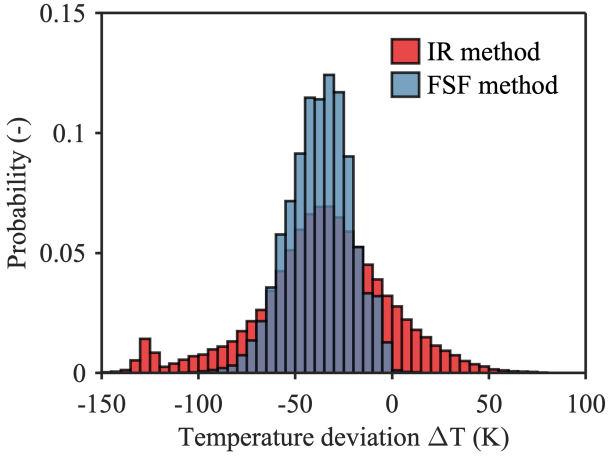


**Fig. 14** Histograms of the temperature deviation $\Delta T = T_{found} - T_{recorded}$. Single-shots are taken at 11 mJ cm$^{-2}$ laser fluence and the database (and the intensity ratio calibration curve) at 106 mJ cm$^{-2}$.

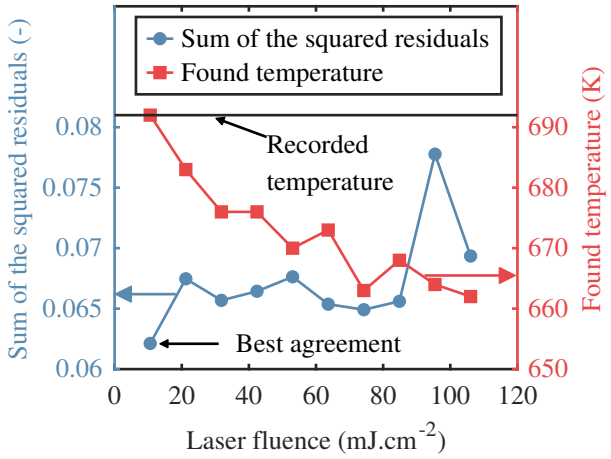


**Fig. 15** Example of minimums of the squared residuals from each databases (blue dots) and associated temperatures (red squares) with FSF method and recorded spectrum temperature (black line) for a single-shot at 11 mJ cm$^{-2}$ laser fluence.

unknown during the measurement, especially when the laser beam must cross a high UV absorbing reactive flow.

• Consequences on temperature determination:

To illustrate the effect of the $Mg_{3.5}FGeO_5$:Mn laser fluence dependence on temperature determination with FSF and IR methods in combustion environments, a scenario where the database (or calibration curve) and the measurements are acquired at different energies is simulated. This scenario replicates an attenuation of 90 % of the incident laser fluence.

The database of spectra and the intensity ratio calibration curve are taken at 106 mJ cm$^{-2}$ and all single-shots measurements at 11 mJ cm$^{-2}$. The FSF method and the IR method are applied for each single-shots. The temperature deviation histograms for both methods are illustrated in figure 14. They show most of the time an underestimated temperature. While the average temperature error is −35 K for both methods, results are more dispersed with the IR method, $\sigma_{\Delta T,\,IR} = 39.08$ K, than with the FSF one, $\sigma_{\Delta T,\,FSF} = 22.87$ K.

• Improved methodology to minimize the effects of the laser fluence:

To reduce the effect of the $Mg_{3.5}FGeO_5$:Mn laser fluence dependence on temperature determination with FSF method, the least mean square algorithm is improved to compare the single-shot spectrum with all the databases for any fluence. Thus, at each laser fluence, a minimum of the sum of the squared residuals is found with a corresponding spectrum and its temperature. An example is shown in figure 15. The temperature is finally given by the minimum of these minimums, 692 K for this example, precisely corresponding to the recorded single-shot temperature.

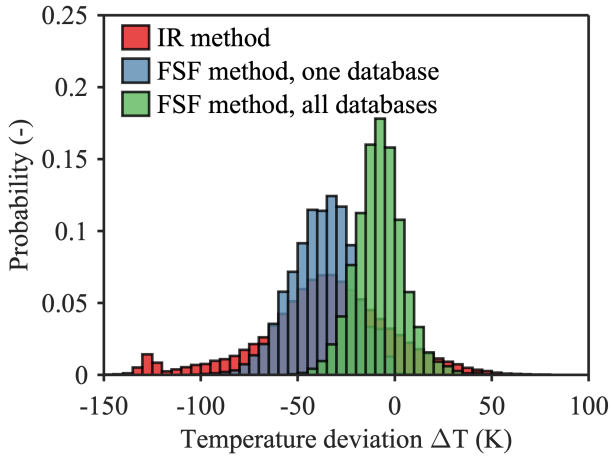


**Fig. 16** Histograms of the temperature deviation $\Delta T = T_{found} - T_{recorded}$. Single-shots are taken at 11 mJ cm$^{-2}$ laser fluence. With the IR method, the calibration curve is taken at 106 mJ cm$^{-2}$.

The same scenario is replayed using the modified data processing for the FSF method. The results are displayed on the temperature deviation histograms in figure 16. The average temperature error is now centered at −8 K with the improved FSF method against −35 K with the previous one. Moreover, results are less dispersed around this average error with a standard deviation of 15.71 K. Unfortunately, the minimum of the sum of squared residuals for all fluences does not always lead to the smallest temperature deviation with the single-shot. This is why the histogram is not centered at 0 K. One of the advantages of the least mean square algorithm is to be easily implemented by everyone. A more advanced comparison algorithm could solve this issue.

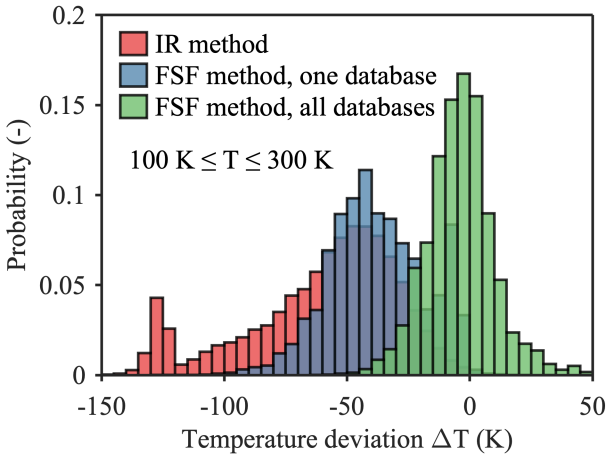


**Fig. 17** Histograms of the temperature deviation $\Delta T = T_{found} - T_{recorded}$ in the range of 100 K to 300 K. Single-shots are taken at 11 mJ cm$^{-2}$ laser fluence. With the IR method, the calibration curve is taken at 106 mJ cm$^{-2}$.

Figure 17 shows the same analysis on the temperature range from 100 K to 300 K, where there is the strongest dependence on the laser fluence. The average temperature error drops to −4 K with the improved FSF method against −39 Kwithout laser fluence consideration. The dispersion is also reduced with a standard deviation of 16.37 K compared to 29.20 K. In contrast, the average temperature error reaches −49 K and the standard deviation 32.28 K with the IR method in this temperature range.

Finally, the modified data processing of the FSF method consisting of checking all databases at different laser fluences is applied to determine the temperature of all the single-shots acquired for this study, regardless of the laser fluence. Likewise, a histogram is obtained (not shown here) and the associated Gaussian fit gives an average error of −0.43 K and a standard deviation of 16.74 K. This standard deviation is even smaller than the smallest one obtained with the IR method, although the laser fluence was known in that case. Nevertheless, it is still preferable to take the database at the same laser fluence when the single-shot fluence is known as statistics are slightly better (figure 11). Once again, this work proves the benefits of taking advantage of the full phosphorescence spectrum and using the FSF method to determine the temperature in harsh environments, especially if the thermographic phosphor used has a laser fluence dependence.

## 6 Guidance for measurements in harsh environments

This section proposes some advice on performing LIP single-shot measurements with the FSF method in combustion experiments.

As for IR and lifetime methods, the choice of the phosphor remains a critical aspect for the FSF method. One should have a rough idea of the temperature range expected in the experiment to select a sensitive phosphor over this range. The dependence on the laser fluence must be investigated in controlled conditions before conducting the measurements. Certainly, a phosphor whit no dependencies is preferred, but the improved FSF method makes it possible to take advantage of a phosphor with a significant dependence on the laser fluence. In this last case, recording as many databases at different laser fluences as possible is recommended. For example, the phosphors YAG:Dy (Goss et al. 1989; Seyfried et al. 2005; Yu et al. 2010), ZnO:Ga and ZnO:Zn (Särner et al. 2008b) or $BaMg_2Al_{10}O_{17}$:Eu (Särner et al. 2008a) can be considered as good candidates for the FSF method due to their high spectral sensitivity over a wide temperature range. Suitable candidates can also be found from the lists of phosphors with spectrally sensitive responses provided in the reviews by Brübach et al. (2013) and Aldén et al. (2011).

The sum of the squared residuals does not contain spectral information, so ambiguous temperature determination may happen with some phosphors. Besides, the deviation caused by potential laser fluence effects can interact or compensate with the temperature dependence. Advanced spectral correlation procedures, e.g., frequency-domain covariance analysis (Lachaux and Musculus 2007) could be suitable in case of ambiguity.

In combustion applications, the thermal radiations from the flame can interfere/overlap with the phosphorescence spectrum. Yet, the telescope-optical fiber assembly focuses on the surface of interest and acts as a spatial filter, so contributions from the flame should be minimal. If the phenomenon persists, a possibility is recording the thermal background by turning off the laser one out of two pulses. The best approach may be to select an adequate phosphor, but it requires an a priori knowledge of the thermal radiations spectrum encountered.

The same experimental setup should be used for the calibration and the actual measurements, although no significant influence except on the signal-to-noise ratio has been identified using a telescope coupled with an optical fiber. The latter is particularly well-adapted for point measurements on experiments with limited optical access and offers the possibility of simultaneous multi-point measurements with a single spectrometer.

## 7 Conclusions

A new approach and post-processing of the Laser Induced Phosphorescence signal have been studied for instantaneous surface temperature measurements: the Full Spectrum Fitting method. The dependence of the entire $Mg_{3.5}FGeO_5$:Mn

phosphorescence spectrum is exploited for single-shot measurements on an 800 K range.

Statistical studies were conducted in well-controlled conditions. The FSF method shows a lower dispersion of the results with no significant influence of the temperature when single-shots and databases are at the same laser fluence in contrast to the IR method. Best of the statistics with the FSF method are obtained at mid-laser fluence value, 64 mJ $cm^{-2}$: the average temperature error is less than 1 K and the precision 12 K for a global analysis. A 10 K precision is even obtained for single-shots between 700 K and 900 K.

A study on the laser fluence shows dependencies on the spectrum, especially at low temperatures, below 500 K, predominantly on the 630 nm emission band. This affects the IR method and can lead to temperature errors of up to a few dozen kelvins if the measurement fluence is unknown, like in high-absorbing environments for example. The FSF method is also affected but optimizing the method by checking different databases at different fluences considerably decreases this error, keeping a 17 K precision.

This method could easily be applied to other phosphors offering good spectral dynamics to reach different temperature ranges.

This methodology has successfully been applied to determine the temperature of several surfaces inside the cryotechnic testbench MASCOTTE during a joint experimental campaign within the LabEM2C / ONERA / CNES / ArianeGroup R&D consortium (Lechner et al. 2022). The harsh conditions reached in MASCOTTE and the short time of operation were perfect challenges for this technique.

**Acknowledgements** This work is part of an ongoing Ph.D. at EM2C laboratory, co-piloted by CNES, the French National Space Agency, and ArianeGroup. The authors would like to particularly thank Marie Theron from CNES and Marie Robcis and Alexandre Barata from ArianeGroup for helpful discussions.

## References

Abou Nada F, Knappe C, Xu X, Richter M, Aldén M (2014) Development of an automatic routine for calibration of thermographic phosphors. Measurement Science and Technology 25(2):025201, https://doi.org/10.1088/0957-0233/25/2/025201

Abou Nada F, Knappe C, Aldén M, Richter M (2016) Improved measurement precision in decay time-based phosphor thermometry. Applied Physics B 122(6):170, https://doi.org/10.1007/s00340-016-6446-4

Abram C, Fond B, Heyes AL, Beyrau F (2013) High-speed planar thermometry and velocimetry using thermographic phosphor particles. Applied Physics B 111(2):155–160, https://doi.org/10.1007/s00340-013-5411-8

Abram C, Fond B, Beyrau F (2015) High-precision flow temperature imaging using ZnO thermographic phosphor tracer particles. Optics Express 23(15):19453–19468, https://doi.org/10.1364/OE.23.019453

Abram C, Fond B, Beyrau F (2018) Temperature measurement techniques for gas and liquid flows using thermographic phosphor tracer particles. Progress in Energy and Combustion Science 64:93–156, https://doi.org/10.1016/j.pecs.2017.09.001

Aldén M, Omrane A, Richter M, Särner G (2011) Thermographic phosphors for thermometry: A survey of combustion applications. Progress in Energy and Combustion Science 37(4):422–461, https://doi.org/10.1016/j.pecs.2010.07.001

Allison SW, Gillies GT (1997) Remote thermometry with thermographic phosphors: Instrumentation and applications. Review of Scientific Instruments 68(7):2615–2650, https://doi.org/10.1063/1.1148174

Arndt CM, Nau P, Meier W (2020) Characterization of wall temperature distributions in a gas turbine model combustor measured by 2D phosphor thermometry. Proceedings of the Combustion Institute https://doi.org/10.1016/j.proci.2020.06.088

Beshears DL, Capps GJ, Cates MR, Simmons CM, Schwenterly SW (1990) Laser-induced fluorescence of phosphors for remote cryogenic thermometry. Fiber Optic Smart Structures and Skins III 1370:365, https://doi.org/10.1117/12.24869

Bizzak DJ, Chyu MK (1994) Rare-earth phosphor laser-induced fluorescence thermal imaging system. Review of Scientific Instruments 65(1):102–107, https://doi.org/10.1063/1.1144780

Brübach J, Dreizler A, Janicka J (2007) Gas compositional and pressure effects on thermographic phosphor thermometry. Measurement Science and Technology 18(3):764–770, https://doi.org/10.1088/0957-0233/18/3/028

Brübach J, Feist JP, Dreizler A (2008) Characterization of manganese-activated magnesium fluorogermanate with regards to thermographic phosphor thermometry. Measurement Science and Technology 19(2):025602, https://doi.org/10.1088/0957-0233/19/2/025602

Brübach J, Pflitsch C, Dreizler A, Atakan B (2013) On surface temperature measurements with thermographic phosphors: A review. Progress in Energy and Combustion Science 39(1):37–60, https://doi.org/10.1016/j.pecs.2012.06.001

Cates MR, Beshears DL, Allison SW, Simmons CM (1997) Phosphor thermometry at cryogenic temperatures. Review of Scientific Instruments 68(6):2412–2417, https://doi.org/10.1063/1.1148125

Cates MR, Allison SW, Jaiswal SL, Beshears DL (2003) YAG:Dy and YAG:Tm Fluorescence Above 1400 C. Pro-

ceedings of the International Instrumentation Symposium 19 https://doi.org/10.2172/885851

Chambers M, Clarke D (2009) Doped Oxides for High-Temperature Luminescence and Lifetime Thermometry. Annual Review of Materials Research 39(1):325–359, https://doi.org/10.1146/annurev-matsci-112408-125237

Degenève A (2020) Stabilization, structure and thermal behavior of oxy-flames with a variable swirl level. PhD thesis, Université Paris-Saclay

Degenève A, Jourdaine P, Mirat C, Vicquelin R, Schuller T (2018) Optimisation de la mesure de température de paroi par thermographie de luminophore appliquée à la combustion. 16ème Congrès Francophone de Techniques Laser pour la mécanique des fluides

Degenève A, Jourdaine P, Mirat C, Caudal J, Vicquelin R, Schuller T (2019) Analysis of wall temperature and heat flux distributions in a swirled combustor powered by a methane-air and a $CO_2$-diluted oxyflame. Fuel 236:1540–1547, https://doi.org/10.1016/j.fuel.2018.09.012

Dramićanin MD (2020) Trends in luminescence thermometry. Journal of Applied Physics 128(4):040902, https://doi.org/10.1063/5.0014825

Feist JP (2001) Development of Phosphor Thermometry for Gas Turbines. PhD thesis, University of London

Fond B, Abram C, Heyes AL, Kempf AM, Beyrau F (2012) Simultaneous temperature, mixture fraction and velocity imaging in turbulent flows using thermographic phosphor tracer particles. Optics Express 20(20):22118, https://doi.org/10.1364/OE.20.022118

Fond B, Abram C, Beyrau F (2015) On the characterisation of tracer particles for thermographic particle image velocimetry. Applied Physics B 118(3):393–399, https://doi.org/10.1007/s00340-014-5997-5

Fuhrmann N, Baum E, Brübach J, Dreizler A (2011) High-speed phosphor thermometry. Review of Scientific Instruments 82(10):104903, https://doi.org/10.1063/1.3653392

Fuhrmann N, Brübach J, Dreizler A (2013) Phosphor thermometry: A comparison of the luminescence lifetime and the intensity ratio approach. Proceedings of the Combustion Institute 34(2):3611–3618, https://doi.org/10.1016/j.proci.2012.06.084

Goss LP, Smith AA, Post ME (1989) Surface thermometry by laser-induced fluorescence. Review of Scientific Instruments 60(12):3702–3706, https://doi.org/10.1063/1.1140478

Guiberti T (2015) Analysis of the topology of premixed swirl-stabilized confined flames. PhD thesis, Ecole Centrale Paris

Guiberti TF, Scouflaire P, Schuller T (2014) La phosphorescence induite par laser pour la mesure de la température des surfaces d'une chambre de combustion. 14ème Congrès Francophone de Techniques Laser pour la mécanique des fluides

Guiberti TF, Durox D, Scouflaire P, Schuller T (2015) Impact of heat loss and hydrogen enrichment on the shape of confined swirling flames. Proceedings of the Combustion Institute 35(2):1385–1392, https://doi.org/10.1016/j.proci.2014.06.016

Heeg B, Jenkins TP (2013) Precision and accuracy of luminescence lifetime-based phosphor thermometry: A case study of eu(iii):ysz. AIP Conference Proceedings 1552(1):885–890, https://doi.org/10.1063/1.4819661

Heichal Y, Chandra S, Bordatchev E (2005) A fast-response thin film thermocouple to measure rapid surface temperature changes. Experimental Thermal and Fluid Science 30(2):153–159, https://doi.org/10.1016/j.expthermflusci.2005.05.004

Hertle E, Bollmann J, Aßmann S, Kalancha V, Osvet A, Batentschuk M, Will S, Zigan L (2020) Characterization of the phosphor (Sr,Ca)SiAlN3: Eu2+ for temperature sensing. Journal of Luminescence p 117487, https://doi.org/10.1016/j.jlumin.2020.117487

Imanaga S, Yokono S, Hoshina T (1979) Luminescence saturation effects in Y2O2S:Eu phosphor. Japanese Journal Of Applied Physics https://doi.org/10.1143/JJAP.19.41

Khalid AH, Kontis K (2008) Thermographic Phosphors for High Temperature Measurements: Principles, Current State of the Art and Recent Applications. Sensors 8(9):5673–5744, https://doi.org/10.3390/s8095673

Kissel T, Baum E, Dreizler A, Brübach J (2009) Two-dimensional thermographic phosphor thermometry using a CMOS high speed camera system. Applied Physics B 96(4):731–734, https://doi.org/10.1007/s00340-009-3626-5

Koren C, Vicquelin R, Gicquel O (2018) Multiphysics Simulation Combining Large-Eddy Simulation, Wall Heat Conduction and Radiative Energy Transfer to Predict Wall Temperature Induced by a Confined Premixed Swirling Flame. Flow, Turbulence and Combustion 101(1):77–102, https://doi.org/10.1007/s10494-018-9895-5

Kueh KCY, Lau T, Nathan GJ, Alwahabi ZT (2015) Temperature Measurements by Laser-induced Phosphorescence: Effect of Laser Flux Variation. 7th Australian Conference on Laser Diagnostics in Fluid Mechanics and Combustion

Lachaux T, Musculus MPB (2007) In-cylinder unburned hydrocarbon visualization during low-temperature compression-ignition engine combustion using formaldehyde PLIF. Proceedings of the Combustion Institute 31(2):2921–2929, https://doi.org/10.1016/j.proci.2006.07.044

Lawrence M, Zhao H, Ganippa L (2013) Gas phase thermometry of hot turbulent jets using laser induced phosphorescence. Optics Express 21(10):12260, https://doi.org/10.1364/OE.21.012260

Lechner V, Betrancourt C, Scouflaire P, Vingert L, Ducruix S (2022) Dynamic characterization of wall temperature in LOX/CH4 rocket engine operating conditions using phosphor thermometry. Proceedings of the Combustion Institute 39 (accepted)

Lempereur C, Andral R, Prudhomme JY (2008) Surface temperature measurement on engine components by means of irreversible thermal coatings. Measurement Science and Technology 19(10):105501, https://doi.org/10.1088/0957-0233/19/10/105501

Lindén J, Takada N, Johansson B, Richter M, Aldén M (2009) Investigation of potential laser-induced heating effects when using thermographic phosphors for gas-phase thermometry. Applied Physics B 96(2-3):237–240, https://doi.org/10.1007/s00340-009-3608-7

Lux J, Suslov D, Bechle M, Oschwald M, Haidn O (2006) Investigation of Sub- and Supercritical LOX/Methane Injection Using Optical Diagnostics. In: 42nd AIAA/ASME/SAE/ASEE Joint Propulsion Conference & Exhibit, https://doi.org/10.2514/6.2006-5077

Marr MA, Wallace JS, Chandra S, Pershin L, Mostaghimi J (2010) A fast response thermocouple for internal combustion engine surface temperature measurements. Experimental Thermal and Fluid Science 34(2):183–189, https://doi.org/10.1016/j.expthermflusci.2009.10.008

McCormack J (1981) Remote optical measurement of temperature using luminescent materials. Electronics Letters 17(18):630, https://doi.org/10.1049/el:19810442

Mendieta A, Fond B, Dragomirov P, Beyrau F (2019) A delayed gating approach for interference-free ratio-based phosphor thermometry. Measurement Science and Technology 30(7):074002, https://doi.org/10.1088/1361-6501/ab1b0c

Mercier R, Guiberti TF, Chatelier A, Durox D, Gicquel O, Darabiha N, Schuller T, Fiorina B (2016) Experimental and numerical investigation of the influence of thermal boundary conditions on premixed swirling flame stabilization. Combustion and Flame 171:42–58, https://doi.org/10.1016/j.combustflame.2016.05.006

Nau P, Yin Z, Geigle KP, Meier W (2017) Wall temperature measurements at elevated pressures and high temperatures in sooting flames in a gas turbine model combustor. Applied Physics B 123(12):279, https://doi.org/10.1007/s00340-017-6856-y

Omrane A, Juhlin G, Aldén M, Josefsson G, Engström J, Benham T (2004a) Demonstration of Two-Dimensional Temperature Characterization of Valves and Transparent Piston in a GDI Optical Engine. SAE Transactions 113:449–457

Omrane A, Juhlin G, Ossler F, Aldén M (2004b) Temperature measurements of single droplets by use of laser-induced phosphorescence. Applied Optics 43(17):3523, https://doi.org/10.1364/AO.43.003523

Petit S, Xavier P, Godard G, Grisch F (2022) Improving the temperature uncertainty of Mg4FGeO6:Mn4+ ratio-based phosphor thermometry by using a multi-objective optimization procedure. Applied Physics B 128(3):57, https://doi.org/10.1007/s00340-021-07733-3

Salgues D, Mouis AG, Lee SY, Kalitan D, Pal S, Santoro R (2006) Shear and Swirl Coaxial Injector Studies of LOX/GCH4 Rocket Combustion Using Non-Intrusive Laser Diagnostics. In: 44th AIAA Aerospace Sciences Meeting and Exhibit, https://doi.org/10.2514/6.2006-757

Seyfried H, Särner G, Omrane A, Richter M, Schmidt H, Aldén M (2005) Optical Diagnostics for Characterization of a Full-Size Fighter-Jet Afterburner. In: Proceedings of the ASME Turbo Expo 2005, pp 813–819, https://doi.org/10.1115/GT2005-69058

Someya S, Uchida M, Tominaga K, Terunuma H, Li Y, Okamoto K (2011) Lifetime-based phosphor thermometry of an optical engine using a high-speed CMOS camera. International Journal of Heat and Mass Transfer 54(17):3927–3932, https://doi.org/10.1016/j.ijheatmasstransfer.2011.04.032

Someya S, Furutani H, Okamoto K (2013) Instantaneous phosphor thermometry applicable to walls exposed to flames. Experimental Thermal and Fluid Science 47:224–231, https://doi.org/10.1016/j.expthermflusci.2013.01.017

Särner G, Richter M, Aldén M (2008a) Investigations of blue emitting phosphors for thermometry. Measurement Science and Technology 19(12):125304, https://doi.org/10.1088/0957-0233/19/12/125304

Särner G, Richter M, Aldén M (2008b) Two-dimensional thermometry using temperature-induced line shifts of ZnO:Zn and ZnO:Ga fluorescence. Optics Letters 33(12):1327, https://doi.org/10.1364/OL.33.001327

Vander Wal RL, Householder PA, Wright TW (1999) Phosphor Thermometry in Combustion Applications. Applied Spectroscopy 53(10):1251–1258, https://doi.org/10.1366/0003702991945498

Vingert L, Ordonneau G, Fdida N, Grenard P (2016) A Rocket Engine under a Magnifying Glass. AerospaceLab (11):15

Yu M, Särner G, Luijten CCM, Richter M, Aldén M, Baert RSG, Goey LPHd (2010) Survivability of thermographic phosphors (YAG:Dy) in a combustion environment. Measurement Science and Technology 21(3):037002, https://doi.org/10.1088/0957-0233/21/3/037002